



A numerical simulation technique to study fault activation characteristics during mining between fault bundles

Huiyong Yin¹ · Shizhen Sang¹ · Daolei Xie¹ · Han Zhao¹ · Shujing Li¹ · Haisong Li¹ · Xuehou Zhuang²

Received: 11 September 2018 / Accepted: 16 February 2019 / Published online: 25 February 2019
© Springer-Verlag GmbH Germany, part of Springer Nature 2019

Abstract

Faults, especially fault bundles, elevate the difficulties of predicting, preventing and controlling water inrush during coal seam mining. This paper takes the no. 163 mining area at Jiangzhuang Coal Mine of Shandong Province, China, as a case study. A series of faults form structural patterns consisting of the graben-horst and fault terrace in the study area. The key technical challenge lies in fault activation, which affects sizing of economic and safe coal-pillar around the fault bundles. An innovative numerical simulation technique was applied to understand the movement law of coal seam roof and floor and fault activation among the fault bundles under different mining plans. The results show that reasonable arrangement of mining sequence in the working faces is an effective method to reduce the influence from faults. In addition, coal seam roof and floor damage and faults activation are different during mining under the graben-horst and fault terrace settings. Moreover, the horizontal and vertical displacement values of each point on fault plane of hanging wall and footwall indicate that the maximum displacement is related to roof water-conducting fractured zone and floor damage zone, which increase the probability of fault activation. Based on the research results, a reasonable coal-pillar width was designed beside the fault bundle in the no. 16301 working face of the no. 163 mining area, and the mining was completed safely with significant economic benefits for Jiangzhuang Coal Mine.

Keywords Coal-pillar width · Fault bundles · Fault activation · Graben-horst · Mine water disaster · Numerical simulation

Introduction

With the coal mining depth increasing in China, more coal mines are threatened by the confined aquifer of the Ordovician limestone under the coal seams during mining for the North China coalfield (Zhang 2005; LaMoreaux et al. 2014; Sun et al. 2016; Yang et al. 2017; Liu et al. 2017), and mine

water inrush accidents occur more frequently (Sun et al. 2015; Xu et al. 2018). Mining in complex areas with faults requires extensive effort (Tan et al. 2012; Wang et al. 2017; Shi et al. 2019; Zhao et al. 2018) because of the increase in the water inrush risk. Approximately 80% water inrushes were related to the faults (Wu et al. 2016; Qiao et al. 2017). Faults complicate the movement and damage characteristics of coal seam roof and floor strata (Tan et al. 2010), mining space stress field characteristics (Sainoki and Mitri 2017), and water inrush pathway evolution and formation. These effects increase the groundwater storage and migration (Huang et al. 2017; Chen et al. 2018; Yin et al. 2018a) and elevate the difficulty of predicting, preventing and controlling water inrush accident. Therefore, fault exploration and identification, fault activation, and fault coal-pillar retention are some of the key issues challenging mine hydrogeological professionals (Guo et al. 2017; Zhang et al. 2017b). Numerical simulation (Cheng et al. 2013; Yin et al. 2016; Zhou et al. 2018), analog simulation (Zhang et al. 2017a), laboratory test (Tan et al. 2011; Zhang et al. 2018), field monitoring (Zhao et al. 2012; Liang et al. 2015; Yin et al.

Electronic supplementary material The online version of this article (<https://doi.org/10.1007/s12665-019-8142-2>) contains supplementary material, which is available to authorized users.

✉ Huiyong Yin
huiyongy@sdust.edu.cn
Daolei Xie
skd994469@sdust.edu.cn

¹ Shandong Provincial Key Laboratory of Depositional Mineralization and Sedimentary Minerals, College of Earth Science and Engineering, Shandong University of Science and Technology, Qingdao 266590, Shandong, China

² Jiangzhuang Coal Mine, Zaozhuang mining (group) Co., Ltd., Zaozhuang 277519, Shandong, China

2015) and theoretical research are commonly used to study fault activation (Qi et al. 2017; Yu et al. 2017). Many useful rules have been obtained and effectively guided safe mining operations (Yin et al. 2018b). However, the strata failure law, faults activation characteristics and pillar width of coal seam mining roof and floor are different in different mining areas where complicated geological and hydrogeological conditions, especially, fault bundles or fault groups are present. Fault bundles may increase the probability of water inrush. Therefore, under the condition of fault bundles, the failure law and activation characteristics of coal seam mining roof and floor need to be further studied and re-evaluated.

In this paper, the no. 163 mining area of Jiangzhuang Coal Mine (CM) in Shandong Province is taken as a case study. Safe exploitation of the coal seam in this mining area requires installation of a coal-pillar at the fault. A numerical simulation technique is provided for investigating the faults activation characteristics, designing the economic and safe pillar width at faults, and guiding the prevention and control of water inrush through fault in the mining area. Numerical simulation technology is often used by engineers and scientists (Yin et al. 2016; Meng et al. 2018) to establish the structural conditions suitable for the fault bundles and simulate the failure of the roof and floor and the fault activation under the condition of coal seam mining. The simulation results provided recommendations on the reasonable width of the coal-pillar.

Study area

Jiangzhuang CM is located at Weishan County, Shandong Province, as shown in Fig. 1. The coalfield is approximately 3.5-km wide from east to west, 10-km long from north to south, with an area of approximately 36 km². Jiangzhuang CM lies between 34°53'24"N and 34°58'18"N latitude and 117°01'12"E and 117°06'54"E longitude.

The lithology is typical of North China coalfield of Permo-Carboniferous coal-bearing age. The mined coal seams are in the Permian Shanxi and Taiyuan formations. The no. 163 mining area is in the central and western part of the coal mine. The mining area is 2700 by 2900 m. The floor elevation of Coal seam Bed no. 16 (CB16) ranges from −400 to −560 m below mean sea level. The buried depth increases gradually from west to east with an average coal seam thickness of 0.89 m. The coal reserves in the mining area are approximately 7.5 million tons. The main aquifers affecting the CB16 mining are no. 10 limestone directly overlying the CB16 and no. 14 limestone and Ordovician limestone underling the CB16. Since the no. 10 and no. 14 limestone is characterized with low-specific water yields, they do not have obvious impacts on the CB16 mining. The Ordovician limestone aquifer is a regional aquifer with a thickness of over 600 m and threatens the CB16 mining. Therefore, this numerical simulation focused on the Ordovician limestone aquifer.

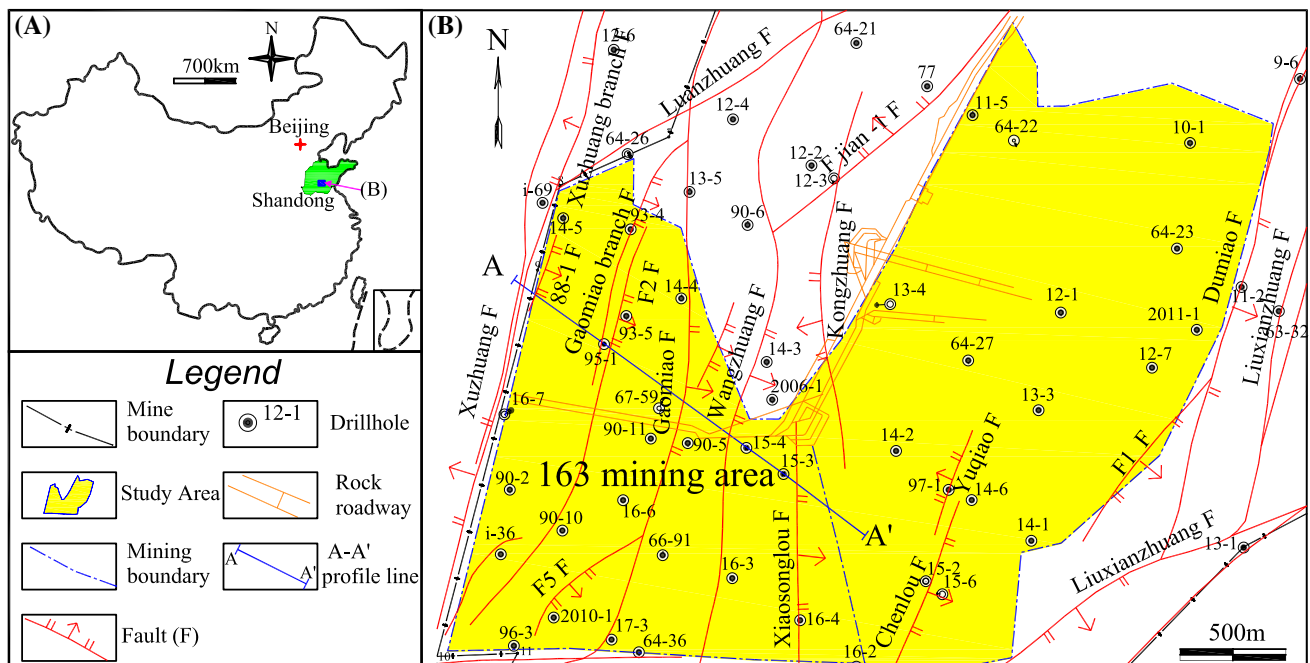


Fig. 1 Location and faults distribution of study area

Figure 1 shows the distribution of faults in the working area. All the faults were identified by three-dimensional seismic exploration, geo-exploration, and roadway and workface extractions. Table 1 summarizes the characteristics of these faults. Obviously, more faults lie in southwest of the no. 163 mining area. Configuration of these faults, also referred to as fault bundles in this paper, form structures of the graben-horst and fault terrace (Fig. 2). These unique structural styles not only increase the difficulty of tunneling but also raise the water inrush risk from the underlying Ordovician limestone aquifer. Furthermore, the water inrush coefficient of the Ordovician limestone aquifer is greater than 0.06 MPa/m in this area,

whereas 0.06 MPa/m is the threshold water inrush coefficient according to the regulations of China State Administration of Coal Mine Safety (2009). In addition, the faults and associated secondary faults tend to turn into water inrush pathways in the graben-horst and fault terrace area. The activation characteristics of the fault bundles have not been studied under mining conditions. The methods recommended in the regulations (State Administration of Coal Mine Safety 2009) are not readily applicable to design of the safe pillar width at the presence of the fault bundles. A three-dimensional geological model is established using the FLAC3D numerical simulation software to study the activation processes of the fault bundles

Table 1 Fault statistics list in study area

No.	Fault name	Type	Occurrence			Fall throw (m)	Length in mining area (m)
			Strike	Dip	Dip angle (°)		
1	88-1 F	Normal	Near SN-NE	E-SE	70	16	378
2	Gaomiao branch F	Normal	NNE	SEE	75	9–32	868
3	F2 F	Normal	NE- NNE	SE- SEE	68–75	20–30	2056
4	F5 F	Normal	NE	SE	75	32	678
5	Gaomiao F	Normal	Near SN	Near EW	60–70	30–80	1740
6	14-7 F	Normal	NE	SE	77	24	225
7	Wangzhuang F	Normal	Near SN	Near EW	50–70	38–90	1225
8	Xiaosonglou F	Normal	SN	EW	75	15–20	1136
9	Kongzhuang F	Normal	SSE	SWW	65–75	10–20	524
10	Yuqiao F	Normal	SW	NW	60	15	520
11	Chenlou F	Normal	NE	SE	56–72	25–40	818
12	F1 F	Normal	NE	SE	70	74	503
13	Dumiao F	Normal	NE	NE	75	70–100	250
14	Xuzhuang F	Normal	NNE	NWW	75	40–90	
15	Xuzhuang branch F	Normal	NNE	NWW	75	60–120	
16	Yuantang F	Normal	EW	S	65–75	45	

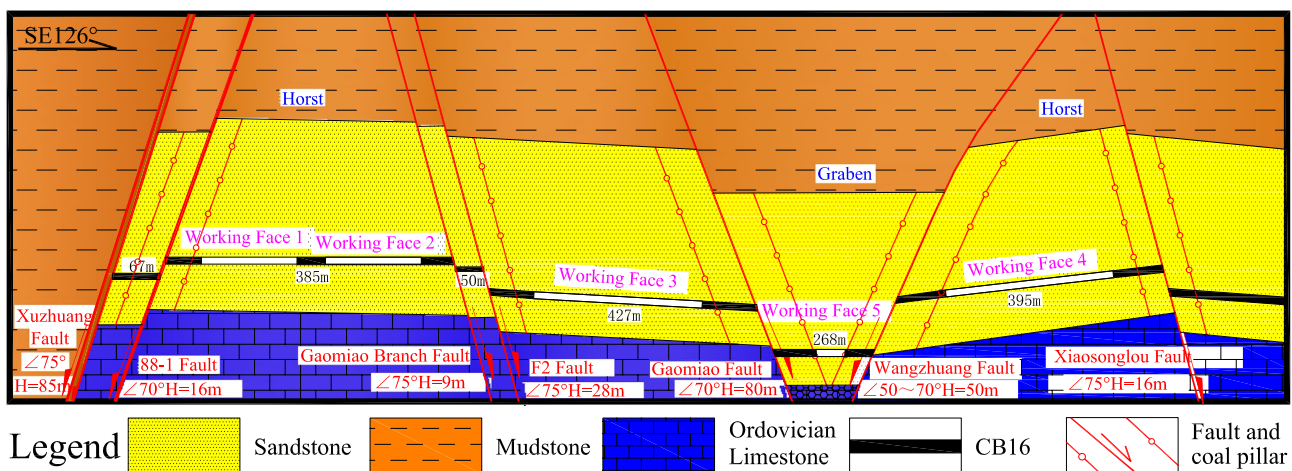


Fig. 2 Fault bundle with graben-horst and fault terrace of A–A’ profile line

under mining conditions. The displacement and block states of the upper and lower parts of the fault bundles and the stress state of the fault surface are simulated under various scenarios. The simulation results provide the technical basis for setting up the reasonable size of the coal-pillar so that a water inrush would not occur.

Numerical simulation technique

FLAC3D, a popular nonlinear three-dimensional numerical simulation software that has been used in many technical fields (Zhu et al. 2014; Yin et al. 2019; Liu et al. 2017), is applied to achieve the simulation objectives with integration of field geological conditions and production technology conditions, field measurements, results of rock physical mechanics test and similarity simulation tests. FLAC3D can simulate the three-dimensional mechanical behavior of geotechnical and other materials. To simulate and observe the variation rules of rock stress in the floor, vertical displacement in the roof and floor, and failure range of roof and floor during the mining process, the local grid was refined where concentrated stress and deformation and failure of roof and floor occur. The failure of rock mass conforms to the Mohr–Coulomb criterion (Yin 2011). The Mohr–Coulomb elastoplastic constitutive model and the Mohr–Coulomb yield criterion were used in this numerical simulation. The Mohr–Coulomb yield criterion is

$$f_c = \sigma_1 - \sigma_3 \frac{1 + \sin \varphi}{1 - \sin \varphi} + 2c \frac{\cos \varphi}{1 - \sin \varphi}, \quad (1)$$

$$f_t = \sigma_3 - \sigma_t, \quad (2)$$

where, σ_1 is the maximum principal stress, Mpa; σ_3 is the minimum principal stress, Mpa; c is the cohesive force, Mpa; φ is the internal friction angle, °; σ_t is the tensile strength, Mpa. When $f_c = 0$, the rock mass will undergo shear failure, and when $f_t = 0$, the rock mass will undergo tension failure (Yin 2011; Lv 2017).

According to Newton's law of motion and Cauchy stress principle, the equation of motion equilibrium can be derived as follows:

$$\frac{\partial \sigma_{ij}}{\partial x_j} + \rho b_i = \rho \frac{dv_i}{dt}, \quad (3)$$

where, σ_{ij} is the stress; X_j is the position vector component of a point; b_i is the physical force; v_i is the velocity; ρ is the particle density; and dt represents the infinitesimal time period.

When the acceleration of the particle is zero, Eq. (3) becomes the static equilibrium equation:

$$\frac{\partial \sigma_{ij}}{\partial x_j} + \rho b_i = 0. \quad (4)$$

The constitutive equation is

$$[\dot{\sigma}]_{ij} = H_{ij}(\sigma_{ij}, \dot{\xi}_{ij}, \kappa), \quad (5)$$

where, $[\dot{\sigma}]$ is the rate of stress change; H represents a specific functional relationship; σ_{ij} is the stress; $\dot{\xi}_{ij}$ is the strain rate component; and κ is the parameter related to the load history.

The stress of normal rock mass is in relative equilibrium state before the coal seam mining. The initial condition and boundary condition are set. The initial equilibrium is calculated, and the equilibrium is judged by the convergence state of the maximum unbalanced force approaching zero. In the initial equilibrium state, the vertical stress is generated by the gravity stress, and the load does not participate in the simulated rock formation transformation. With the increase of the burial depth of rock mass, the vertical stress increases linearly. In the absence of structure, the vertical initial stress is basically horizontal. However, in the fault area, the initial stress will be affected by the structure. The initial stress is not evenly distributed horizontally, but the vertical stress still increases with the burial depth. According to the strata conditions and coal seam mining conditions, a mechanical concept excavation model is established. The boundary conditions of the model were set as follows: the four sides of the model limit the horizontal movement and no additional stress is applied; the top and bottom of the model limits the vertical movement; and the upper part of the model exerts vertical load instead of the weight of overlying strata.

In the process of modeling, the strata with similar lithology and mechanical parameters are combined. Based on the structural styles as shown in Fig. 2, a model is established and has dimensions of 2330 m long, 300 m wide, and 653 m high. Rock strata above the top of the model are replaced by loads. Figure 3 shows the three-dimensional model, which consists of 220,650 cells and 246,816 nodes.

According to the geological conditions, fault distribution and mining design scheme of the no. 163 mining area, five working faces were designed among the graben-horst and fault terrace (Fig. 2). Two working faces (nos. 1 and 2 working faces) are 150-m wide and between the no. 88-1 Fault (F) and Gaomiao branch F. The no. 3 working face was 200-m wide between the no. F2 F and the Gaomiao F. The no. 5 working face is 100-m wide and located between Gaomiao F and Wangzhuang F. The no. 4 working face is 200 m in wide and located between Wangzhuang F and Xiaosongzhuang F. Excavation was carried out according to the design sequence of working faces. The mining length is 300 m for each working face. The three-dimension simulation model consisting of graben-horst and fault terrace analyzed and summarized the characteristics of roof and floor displacement, block states, and stress within the range of fault bundles, especially the block state to reveal the fault activation characteristics with different working face mining sequence relative to fault bundle, graben-horst and fault terrace.

Results and analysis

Analysis of fault activation characteristics with working face advancement

The working face advancement direction is designed to be consistent with strike of the fault plane during the simulations. The range of damage and fault activation on the fault plane continues to expand as the working face advances.

At the same time, the stress state on the fault plane also changes. The vertical stress distribution and plastic zone of the no. 88-1 F planes during the no. 1 working face excavation are shown in Figs. 4 and 5, respectively. The stress level increased in the area near the goaf on the fault plane when the working face was at 20 m. No plastic failure zone has developed on the fault plane at this time. The areas of stress increasing zone and the plastic failure zone extended throughout the entire excavation when the working face

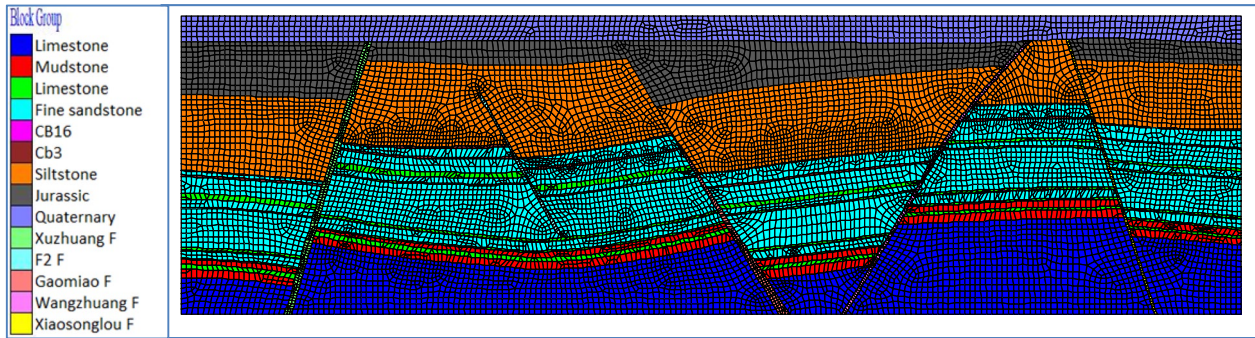


Fig. 3 3D frid model of A–A' line

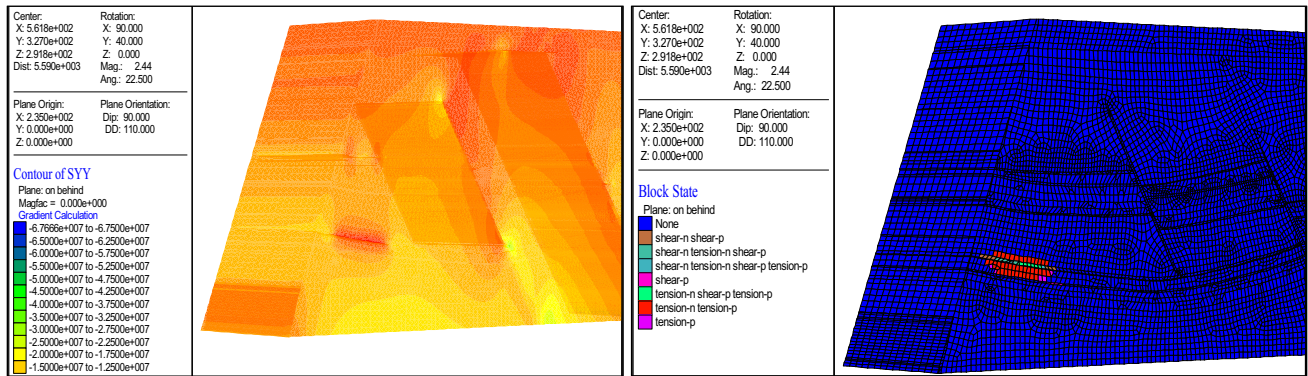


Fig. 4 Vertical stress distribution and plastic zone diagram with mining 20 m at working face 1

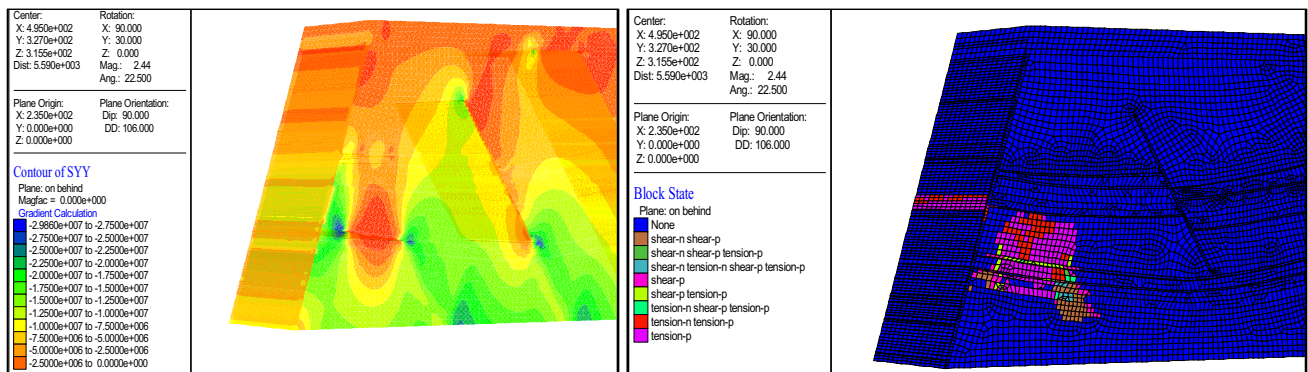


Fig. 5 Vertical stress distribution and plastic zone diagram with mining 300 m at working face 1

advanced to the end at 300 m. The range of the plastic failure zone was on the fault plane. The floor also had the stress increasing zone farthest from the fractured water-flowing zone. However, under the horst condition, the tensile strength produced by cohesive force of coal seam roof was small. The roof was more easily damaged than the coal seam floor and tended to develop a damage and activation zone.

Influence of different working face mining sequence on fault bundle activation

The mining sequence of these working faces affects the stress distribution and the fault status (Zhang et al. 2018). To obtain the influence of working face mining sequence on fault bundle activation, two working faces are designed between 88-1 F and Gaomiao branch F, and they are named as no. 1 working face and no. 2 working face, respectively (Fig. 2). The no. 1 and no. 2 working faces were simulated at first mining, and the results are shown in Figs. 6 and 7, respectively. When the mining started with no. 1 working

face, the stress value in the same area on the no. 88-1 fault and the stress concentration value at both ends of the no. 1 working face were bigger than the stress value at the same position when the mining started with no. 2 working face. The range of the plastic failure zone was relatively large in the top and bottom of 88-1 F as well as the highest site away from the fractured water-flowing zone of no. 1 working face. On the other hand, when the mining started with no. 2 working face, the stress value in the same area on the Gaomiao branch F and the stress concentration value at both ends of the no. 2 working face were bigger than the stress value at the same position when the mining started with no. 1 working face. The range of the plastic failure zone was relatively large in the top and bottom of Gaomiao branch F as well as the highest site away from roof water-conducting fracture zone of the no. 2 working face. The fault near the first mining face was damaged severely during continuous mining in multiple working faces. The simulation results suggest that the influence on faults can be reduced by rationally arranging the working face sequence, thereby reducing the threat from faults.

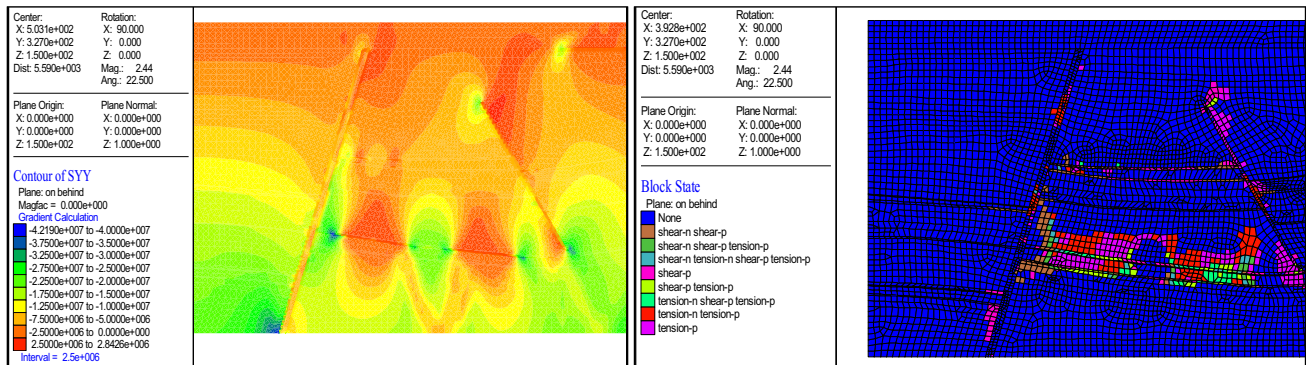


Fig. 6 Vertical stress distribution and plastic zone diagram of working face 1 mined before working face 2

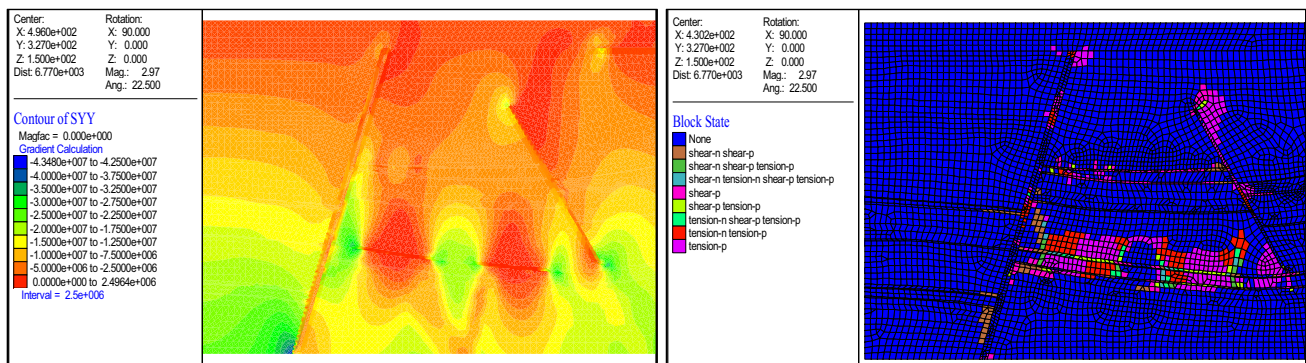


Fig. 7 Vertical stress distribution and plastic zone diagram of working face 1 mined behind working face 2

Fault activation characteristics of fault bundle with graben-horst and fault terrace

A series of fault bundle form several structural styles of graben-horst and fault terrace in the no. 163 mining area, as shown in Fig. 2. The various structural styles influence coal seam mining to different degrees, depending on excavation location relevant to the structures. Coal seam excavation can be on footwall of both faults in graben structure, on hanging wall of both faults in horst structure, or on the fault hanging wall and footwall at each side in the fault terrace. Different location of coal seams mining causes different stress effect and damage law and fault activation characteristics.

The different fault activation characteristics during CB16 mining were studied by simulating mining process for a working face at each location of graben, horst and fault terrace structure. Figures 8, 9 and 10 show the vertical stress distribution and plastic zone during coal seam excavation at the graben, horst and fault terrace structure, respectively. When the coal seam excavation was at the graben structure, the plastic zone of the fault near the floor at both ends of the working face goaf was larger, the damage was severe, and

the activation failure degree of the roof fault was relatively low (Fig. 8). When CB16 excavation was in the horst structure area, the plastic zone of the fault located near the floor at both ends of the goaf was smaller, and the failure and activation were less severe. The fault activation and failure degree at the largest distance position to the roof mining-induced fractured zone was relatively large (Fig. 9). These observations are consistent with findings from Wang et al. (2017). Figure 10 shows that the coal seam mining at the fault terrace structure. When the working face was on the hanging wall of the fault, the fault activation degree of the working face roof was small at the largest distance position to the roof water-conducting fracture zone, whereas the degree of activation and destruction of the floor fault was large. When the working face was on the footwall of the fault, the fault activation degree of the working face roof was large at the largest distance position to the water-flowing fractured zone. The degree of activation and destruction of the floor fault was relatively small.

Different degrees of failure activation under the three scenarios indicate that when the mining is on the fault hanging wall, the fault activation and failure degree are relatively low

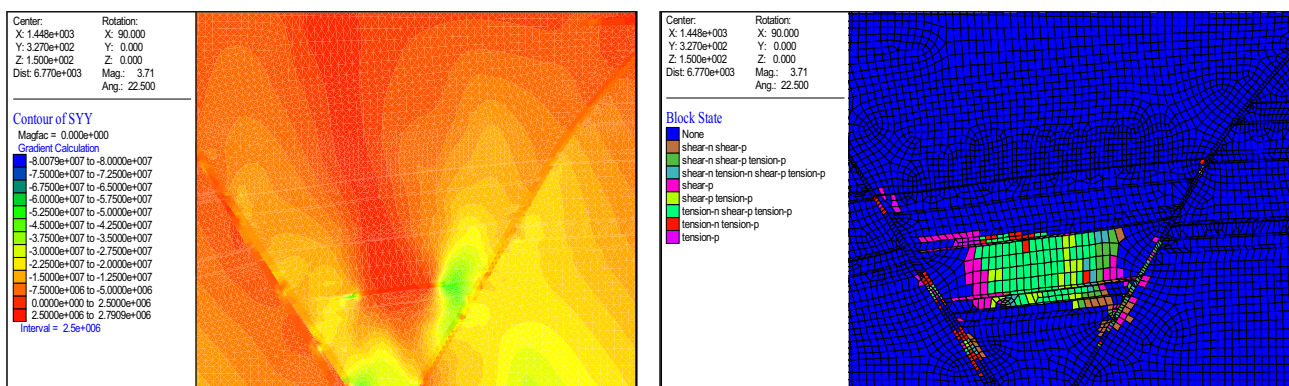


Fig. 8 Vertical stress distribution and plastic zone diagram in graben area

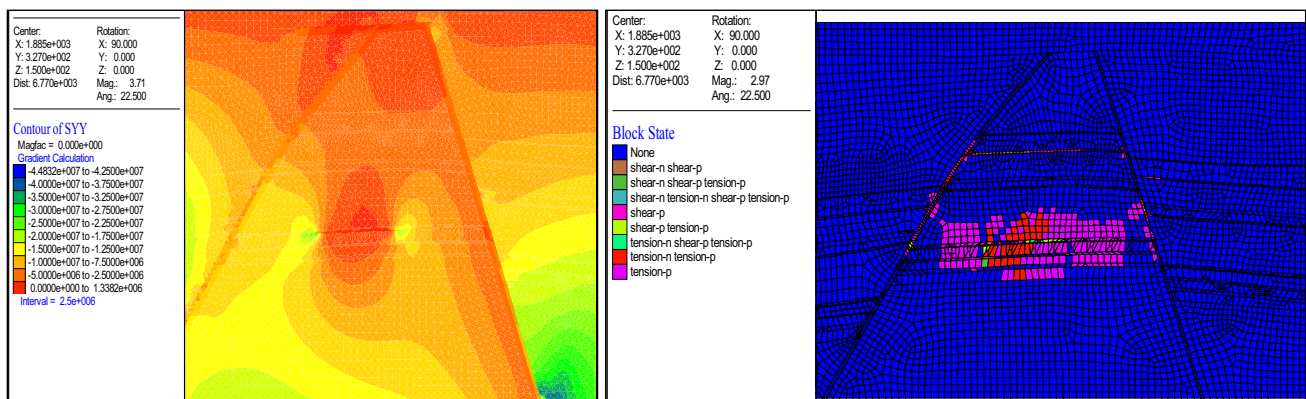


Fig. 9 Vertical stress distribution and plastic zone diagram in horst area

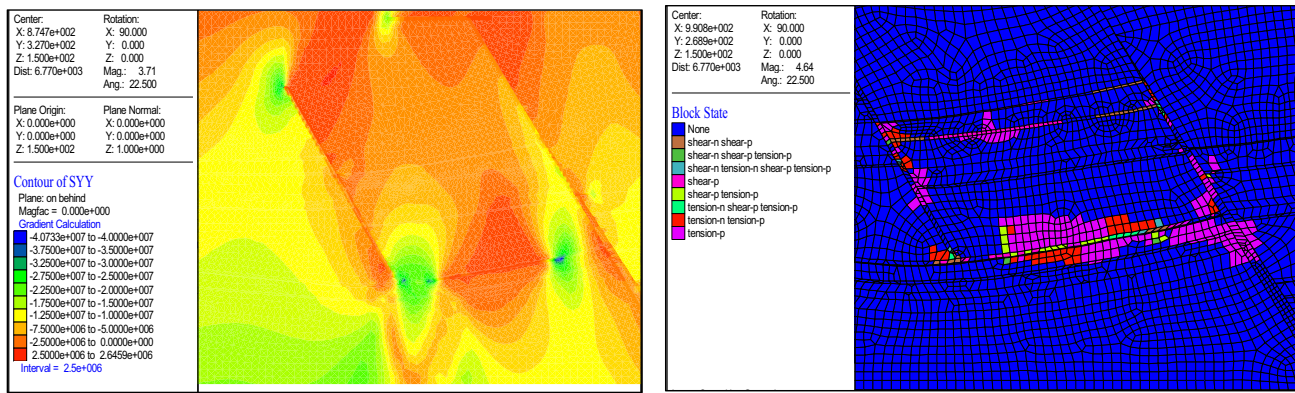


Fig. 10 Vertical stress distribution and plastic zone diagram in fault terrace area

at the largest position to the roof water-conducting fracture zone, and the activation and failure of the fault location are serious near the floor at both ends of the goaf. When the working face excavation is on the fault footwall, the fault activation and failure degree are serious at the largest position to the roof water-conducting fracture zone and the activation and failure of the fault location are relatively low near the floor at both ends of the goaf.

Displacement judgment of fault bundle activation

One monitoring line (Fig. 11) is set on the hanging wall and footwall of each fault plane to extract the horizontal and vertical displacement values at discrete points in response to CB16 mining and to plot the horizontal and vertical displacement curves of the hanging wall and footwall in each fault. Figure 12 shows the displacement changes after taking the horizontal and vertical displacement contrast curves on no. 88-1 F. The horizontal and vertical displacements of the fault planes on the hanging wall and footwall of the fault demonstrate unsynchronized changes in local positions, making the local relative displacement values exist. In areas where the curves do not coincide, i.e., the relative

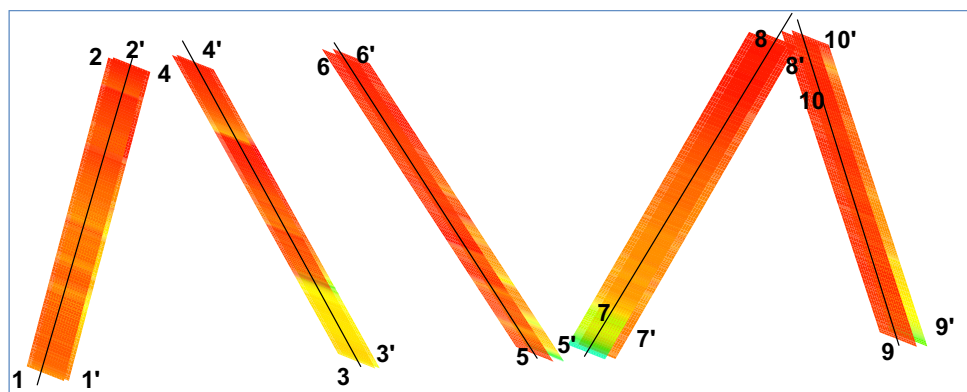
displacement exists, the fault is considered to be activated. It can be seen that all the fault activations occur near the largest water-flowing fractured zone of the goaf roof and the failure zone of the floor where the vertical displacement is relatively large. Fault activation occurs in the fault location where the separation occurs from the bending zone of the roof, and the relative horizontal displacement value of these locations is relatively large.

Based on the above analysis, the following observations are made:

- for the step fault, the fault plane of the floor in the fault hanging wall is easier to be damaged and activated than that of the roof, whereas the fault plane of the roof in the fault footwall is easier to be damaged and activated than that of the floor;
- the fault plane of the floor in the graben structure is easier to be damaged and activated than that of the roof; and
- the fault plane of the roof in the horst structure is easier to be damaged and activated than that of the floor.

At the presence of the fault bundle, the degree of influence of each fault on coal seam mining is related to the size

Fig. 11 Displacements monitoring line on hanging wall and footwall of each fault



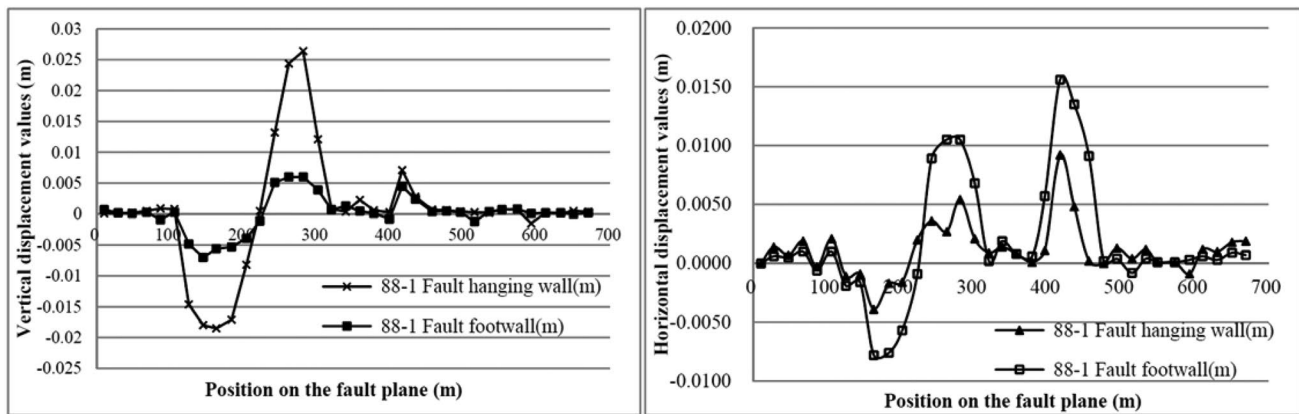


Fig. 12 Vertical (left) and horizontal (right) displacements values on hanging wall and footwall of 88-1 F

of the faults. Larger fault throw and strike cause greater scope of the fault influence and more serious harm to the mine safety. Therefore, it is essential to choose the appropriate mining method to reduce the disturbance and influence of the mining to the faults, and design a reasonable coal-pillar width at the fault bundle.

Application

Setting of fault coal-pillars in China's coal mines generally follows the method recommended in the "Regulations of preventing water hazards for coalmines" (State Administration of Coal Mine Safety 2009). Based on the state-recommended method, the calculated widths range from 38 to 61 m at the Xuzhuang branch F. However, the numerical simulation results suggest a coal-pillar width of 30 m at the same fault. The fault coal-pillar width was set at 30 m in actual mining, and the coal seam was mined safely. Reduction in the coal-pillar width has liberated approximately 250,000 tons of coal, equivalent to 170 million Chinese Yuan.

Conclusion

A series of faults or fault bundles form unique structural styles of graben-horst and fault terrace in the no. 163 mining area of Jiangzhuang CM. Their presence impacts the design in fault coal-pillars, the arrangement of working faces and mining sequence as well as the failure height of coal seam roof and floor during mining. Ultimately, they affect the water inrush risk of the Ordovician limestone aquifer under coal seam floor. A numerical simulation technology is applied to understand the movement law of coal seam roof and floor between the fault bundles under different mining plans.

Under the condition of continuous mining in several working faces, the simulations suggest that the faults near the first mining face are damaged the most. To reduce the threat of fault to safety mining, the influence of faults can be reduced by arranging the working sequence.

The position of the fault plane of the floor in the hanging wall of fault terrace is easier to be damaged and activated than coal seam roof. The position of the fault plane of the roof in the footwall is easier to be damaged and activated than coal seam floor. The position of the fault plane of the floor in the graben structure is easier to be damaged and activated than coal seam roof. The position of the fault plane of the roof in the horst structure is easier to be damaged and activated than coal seam floor.

The horizontal and vertical displacements of each point on the mining monitoring line of the fault plane of hanging wall and footwall indicate that the relatively large vertical displacements are closer to the maximum water-flowing fractured zone of the goaf roof and closer to the floor damage zone. These two locations have increased probability of fault activation.

Acknowledgements This research was financially supported by National Key R&D Program of China (No. 2017YFC0804101) and National Natural Science Foundation of China (Nos. 41402250 and 41702305), and Graduate Science and Technology Innovation Project of Shandong University of Science and Technology (No. SDK-DYC180319), and Taishan Scholar Talent Team Support Plan for Advantaged & Unique Discipline Areas. The authors would like to thank technicians in Department of Geology and Survey in Jiangzhuang Coal Mine. We thank anonymous reviewers for constructive comments on the draft, which greatly benefited the manuscript.

References

- Chen T, Clauser C, Marquart G, Willbrand K, Hiller T (2018) Upscaling permeability for three-dimensional fractured

- porous rocks with the multiple boundary method. *Hydrogeol J* 26(6):1903–1916. <https://doi.org/10.1007/s10040-018-1744-z>
- Cheng JL, Sun XY, Zheng G, Gao F, Kong X, Zhou J (2013) Numerical simulations of water-inrush induced by fault activation during deep coal mining based on fluid-solid coupling interaction. *Disaster Adv* 6(11):10–14
- Guo WJ, Zhao JH, Yin LM, Kong DZ (2017) Simulating research on pressure distribution of floor pore water based on fluid-solid coupling. *Arab J Geosci* 10(1):5–18. <https://doi.org/10.1007/s12517-016-2770-6>
- Huang N, Jiang YJ, Liu RC, Li B (2017) Estimation of permeability of 3-d discrete fracture networks: an alternative possibility based on trace map analysis. *Eng Geol* 226:12–19. <https://doi.org/10.1016/j.enggeo.2017.05.005>
- LaMoreaux JW, Wu Q, Zhou WF (2014) New development in theory and practice in mine water control in China. *Carbonate Evaporite* 29(2):141–145. <https://doi.org/10.1007/s13146-014-0204-7>
- Liang DX, Jiang ZQ, Guan YZ (2015) Field research: measuring water pressure resistance in a fault-induced fracture zone. *Mine Water Environ* 34(3):320–328. <https://doi.org/10.1007/s10230-014-0323-3>
- Liu SL, Liu WT, Yin DW (2017) Numerical simulation of the lagging water inrush process from insidious fault in coal seam floor. *Geotech Geol Eng* 35(3):1–9. <https://doi.org/10.1007/s10706-016-0156-x>
- Lv ZH (2017) Research on mechanism and instability control of coal-rock mass due to mining disturbance near fault zone. Doctor's Thesis, Xi'an University of Science and Technology (Chinese)
- Meng XX, Liu WT, Mu DR (2018) Influence analysis of mining's effect on failure characteristics of a coal seam floor with faults: a numerical simulation case study in the Zhaolou Coal Mine. *Mine Water Environ* 37(4):754–762. <https://doi.org/10.1007/s10230-018-0532-2>
- Qi YM, Li MZ, Li KJ, Yeh T-CJ (2017) Spatiotemporal development of mine water inrush and its mechanism—a case study in Ganhe coal mine, Shanxi, China. *Arab J Geosci* 10(19):433. <https://doi.org/10.1007/s12517-017-3216-5>
- Qiao W, Li WP, Li T, Chang JY, Wang QQ (2017) Effects of coal mining on shallow water resources in semiarid regions: a case study in the Shennan mining area, Shaanxi, China. *Mine Water Environ* 36(1):104–113. <https://doi.org/10.1007/s10230-016-0414-4>
- Sainoki A, Mitri HS (2017) Influence of mining activities on the reactivation of a footwall fault. *Arab J Geosci* 10(5):99. <https://doi.org/10.1007/s12517-017-2913-4>
- Shi SQ, Wei JC, Xie DL, Yin HY, Li LY (2019) Prediction analysis model for groundwater potential based on set pair analysis of a confined aquifer overlying a mining area. *Arab J Geosci* 12:115. <https://doi.org/10.1007/s12517-019-4267-6>
- State Administration of Coal Mine Safety (2009) Regulations of preventing water hazards for coalmines. Coal Industry Press, Beijing (Chinese)
- Sun WJ, Wu Q, Liu HL, Jiao J (2015) Prediction and assessment of the disturbances of the coal mining in Kailuan to karst groundwater system. *Phys Chem Earth* 89–90:136–144. <https://doi.org/10.1016/j.pce.2015.10.008>
- Sun WJ, Zhou WF, Jiao J (2016) Hydrogeological classification and water inrush accidents in China's coal mines. *Mine Water Environ* 35(2):214–220. <https://doi.org/10.1007/s10230-015-0363-3>
- Tan YL, Zhao TB, Xiao YX (2010) In situ investigations of failure zone of floor strata in mining close distance coal seams. *Int J Rock Mech Min* 47(5):865–870. <https://doi.org/10.1016/j.ijrmm.2009.12.016>
- Tan YL, Zhang Z, Zhao TB (2011) AE pattern of rock burst disaster induced by strata activation in coal mine. *Disaster Adv* 4(4):29–33
- Tan YL, Ning JG, Li HT (2012) In situ explorations on zonal disintegration of roof strata in deep coalmines. *Int J Rock Mech Min* 49:113–124. <https://doi.org/10.1016/j.ijrmm.2011.11.015>
- Wang G, Wu MM, Wang R, Xu H, Song X (2017) Height of the mining-induced fractured zone above a coal face. *Eng Geol* 216:140–152. <https://doi.org/10.1016/j.enggeo.2016.11.024>
- Wu Q, Guo XM, Shen JJ, Xu S, Liu SQ, Zeng YF (2016) Risk assessment of water inrush from aquifers underlying the Gushuyuan coal mine, China. *Mine Water Environ* 36(1):1–8. <https://doi.org/10.1007/s10230-016-0410-8>
- Xu ZM, Sun YJ, Gao S, Zhao XM, Duan RQ, Yao MH, Liu Q (2018) Groundwater source discrimination and proportion determination of mine inflow using ion analyses: a case study from the Longmen coal mine, Henan Province, China. *Mine Water Environ* 37:385–392. <https://doi.org/10.1007/s10230-018-0512-6>
- Yang BB, Sui W L Duan (2017) Risk assessment of water inrush in an underground coal mine based on GIS and fuzzy set theory. *Mine Water Environ* 36(4):617–627. <https://doi.org/10.1007/s10230-017-0457-1>
- Yin LM (2011) Basic experimental study on water-inrush mechanism of floor in deep mining. Doctor's Thesis, Shandong University of Science and Technology (Chinese)
- Yin SX, Zhang JC, Liu DM (2015) A study of mine water inrushes by measurements of in situ stress and rock failures. *Nat Hazards* 79(3):1961–1979. <https://doi.org/10.1007/s11069-015-1941-1>
- Yin HY, Wei JC, Lefticariu L, Guo JB, Xie DL, Li ZL, Zhao P (2016) Numerical simulation of water flow from the coal seam floor in a deep longwall mine in China. *Mine Water Environ* 35(2):1–10. <https://doi.org/10.1007/s10230-016-0385-5>
- Yin HY, Shi YL, Niu HG, Xie DL, Wei JC, Lefticariu L, Xu SX (2018a) A GIS-based model of potential groundwater yield zonation for a sandstone aquifer in the Juye Coalfield, Shandong, China. *J Hydrol* 557:434–447. <https://doi.org/10.1016/j.jhydrol.2017.12.043>
- Yin HY, Zhou WF, LaMoreaux JW (2018b) Water inrush conceptual site models for coal mines of China. *Environ Earth Sci* 77:746. <https://doi.org/10.1007/s12665-018-7920-6>
- Yin HY, Zhao H, Xie DL, Sang SZ, Shi YL, Tian MH (2019) Mechanism of mine water inrush from overlying porous aquifer in quaternary: a case study in Xinhe Coal Mine of Shandong Province, China. *Arab J Geosci*. <https://doi.org/10.1007/s12517-019-4325-0>
- Yu B, Zhao J, Xiao HT (2017) Case study on overburden fracturing during longwall top coal caving using microseismic monitoring. *Rock Mech Rock Eng* 50(2):507–511. <https://doi.org/10.1007/s00603-016-1096-8>
- Zhang JC (2005) Investigations of water inrushes from aquifers under coal seams. *Int J Rock Mech Min* 42(3):350–360. <https://doi.org/10.1016/j.ijrmm.2004.11.010>
- Zhang SC, Guo WJ, Li YY (2017a) Experimental simulation of water-inrush disaster from the floor of mine and its mechanism investigation. *Arab J Geosci* 10(22):503–513. <https://doi.org/10.1007/s12517-017-3287-3>
- Zhang SC, Guo WJ, Li YY, Sun WB, Yin DW (2017b) Experimental simulation of fault water inrush channel evolution in a coal mine floor. *Mine Water Environ* 36(3):1–9. <https://doi.org/10.1007/s10230-017-0433-9>
- Zhang WJ, Li SC, Wei JC, Zhang QS, Liu RT, Zhang X, Yin HY (2018) Grouting rock fractures with cement and sodium silicate grout conclusions. *Carbonate Evaporite* 33:211–222. <https://doi.org/10.1007/s13146-016-0332-3>
- Zhao TB, Yin YW, Tan YL (2012) Safe mining and new prediction model in coal seam with rock burst induced by roof. *Disaster Adv* 5(4):961–965
- Zhao TB, Guo WY, Tan YL, Yin YC, Cai LS, Pan JF (2018) Case studies of rock bursts under complicated geological conditions

- during multi-seam mining at a depth of 800 m. *Rock Mech Rock Eng* 51:1539–1564. <https://doi.org/10.1007/s00603-018-1411-7>
- Zhou QD, Herrera J, Hidalgo A (2018) The numerical analysis of fault-induced mine water inrush using the extended finite element method and fracture mechanics. *Mine Water Environ* 37(4):1–11. <https://doi.org/10.1007/s10230-017-0461-5>
- Zhu B, Wu Q, Yang JW, Cui T (2014) Study of pore pressure change during mining and its application on water inrush prevention: a numerical simulation case in Zhaogezhuang coalmine, China.

Environ Earth Sci 71(5):2115–2132. <https://doi.org/10.1007/s12665-013-2616-4>

Publisher's Note Springer Nature remains neutral with regard to jurisdictional claims in published maps and institutional affiliations.